ADVANCED ELECTRONIC MATERIALS
www.advelectronicmat.de

Interlayers for Improved Hole Injection in Organic Field-Effect Transistors

Ke Zhang, Naresh B. Kotadiya, Xiao-Ye Wang, Gert-Jan A. H. Wetzelaer, Tomasz Marszalek, Wojciech Pisula,* and Paul W. M. Blom**

Efficient charge-carrier injection is a critical requirement for high-performance organic electronic devices, such as light-emitting diodes, solar cells, and field-effect transistors. In this work, a significantly improved charge-carrier injection from high work-function metal-oxide electrodes in organic field effect transistors (OFETs) is demonstrated for amorphous organic semiconductors (OSCs) by using organic interlayers with a high ionization energy (IE). Molybdenum oxide (MoO_3) exhibits limited injection into amorphous 2,2′,7,7′-tetrakis(*N*,*N*-diphenylamino)-9,9-spirobifluorene (Spiro-TAD) and tris(4-carbazoyl-9-ylphenyl)amine (TCTA) active layers, resulting in high contact resistance and threshold voltage. By inserting an interlayer of a few nanometers thick with high IE between the MoO_3 electrode and the amorphous OSC films, the Spiro-TAD and TCTA OFETs show a substantial enhancement in hole current, subthreshold swing, and effective charge carrier mobility due to the decreased contact resistance. However, for discontinuous interlayers formed on distinct grain domains as in the case of polycrystalline 2,7-dioctyl[1]benzothieno[3,2-*b*][1]benzothiophene (C8-BTBT) films, the effect of the interlayer reduces. These results demonstrate that the utilization of smooth interlayers with IE higher than the semiconductor is a general approach to elevate the hole injection into amorphous OSCs with high IE in OFETs.

1. Introduction

Organic semiconductors (OSCs) have attracted great attention due to their high potential for light-weight and flexible electronics.[1] Recent efforts in the development of organic field effect transistors (OFETs) have led to significant improvement of the charge carrier mobility from 0.1 to above 10 $cm^2\ V^{-1}\ s^{-1}$, that is comparable to amorphous silicon thin film transistors.[2] For instance, single crystals of 2,7-dioctyl[1]benzothieno[3,2-*b*][1]benzothiophene (C8-BTBT) and 5,7,12,14-tetraazapentacene (TIPS-TAP) show hole and electron mobilities above 10 $cm^2\ V^{-1}\ s^{-1}$.[3,4] However, in contrast to the low contact resistance (R_c) in inorganic thin film transistors, OFETs typically suffer from high R_c since the electrode–OSC junctions consist of a heterogeneous material interface between metal electrode and OSC active film.[5]

The charge injection in OFETs is a critical factor determining the subthreshold swing (SS) and operation voltage. Therefore, various strategies have been proposed to reduce R_c and in this way to improve the charge carrier injection in OFETs.[5–7] One approach is based on the modification of the work-function of the metal electrodes by self-assembled monolayers (SAMs), accomplished by the formation of dipole layers causing shifting of vacuum level.[6] The commonly used SAMs on Au and Ag for tuning charge injection include alkane terminals (decrease of work-function) and terminals with halogen atoms (increase of work-function).[5,8] For instance, 1*H*,1*H*,2*H*,2*H*-perfluoro-decanethiol raised the work-function of Au (4.9 eV) by 0.6 to 5.5 eV, whereas hexadecanethiol decreased it by 0.8 eV.[8]

An alternative method to improve charge carrier injection in OFETs is inserting a doped layer at the interface between electrode and active OSC film.[3] The strong band bending in the doped layer allows charge injection via tunneling.[5] A typical organic p-type dopant such as hexafluorotetracyanonaphthoquinodimethane (F6TCNNQ) has an electron affinity of ≈5.6 eV allowing effective injection into OSCs with an ionization energy (IE) lower than 5.6 eV.[9] As another example, iron(III)trichoride ($FeCl_3$) shows strong oxidation and is also widely used as a dopant.[10] Insertion of $FeCl_3$ into the contact interface of Au

Dr. K. Zhang, Dr. N. B. Kotadiya, Dr. G.-J. A. H. Wetzelaer, Dr. T. Marszalek, Prof. W. Pisula, Prof. P. W. M. Blom
Max Planck Institute for Polymer Research
Ackermannweg 10, Mainz 55128, Germany
E-mail: marszalek@mpip-mainz.mpg.de; pisula@mpip-mainz.mpg.de; blom@mpip-mainz.mpg.de

Dr. X.-Y. Wang
State Key Laboratory of Elemento-Organic Chemistry
College of Chemistry
Nankai University
Tianjin 300071, China

Dr. T. Marszalek, Prof. W. Pisula
Department of Molecular Physics
Faculty of Chemistry
Lodz University of Technology
Zeromskiego 116, Lodz 90-924, Poland

The ORCID identification number(s) for the author(s) of this article can be found under https://doi.org/10.1002/aelm.201901352.

DOI: 10.1002/aelm.201901352

electrode and C8-BTBT film leads to a significant reduction of R_c from 200×10^3 to 8.8×10^3 Ω cm at a gate voltage of −40 V. The improved charge injection is attributed to a reduction in the depletion layer thickness at the contact interface and the occupation of trap states in the access region.

Metal-oxide electrodes, such as molybdenum oxide (MoO_3), are also applied as hole injection layers in organic electronics, owing to their extremely high work-function of 6.7–7.0 eV.[11] The insertion of MoO_3 between Au electrodes and C8-BTBT active film in OFETs lowers the injection barrier height and SS.[12,13] However, in hole-only diodes with sandwich electrode geometry, MoO_3 gives rise to a considerable injection barrier (≈0.4 eV) when contacted with OSCs.[14] In diodes with amorphous hole-transport OSCs, the injection barrier at the MoO_3 electrode gives rise to a considerable limitation of the injected hole current. Interestingly, the injected current greatly improves by inserting a 5 nm interlayer (IL) of another organic semiconductor with an even higher IE than the hole-transport material. As such, an Ohmic contact is formed between the MoO_3 electrode and the hole-transport material, stemming from electrostatic decoupling of the electrode and the organic semiconductor. As a result, the injection barrier formed by electrostatic effects leading to broadening of the density of states (DOS) at the interface is circumvented, while restoring Fermi-level alignment.[14] A high hole density at the organic/organic interface, which plays the role of a virtual Ohmic hole contact, is spatially separated from the electrode by the interlayer. Also for inorganic semiconductors tunneling barriers have been applied since many decades to avoid pinning of the Fermi level of the electrode by interface states of the semiconductor.[15] These findings motivated us to transfer this strategy to the hole injection in OFETs.

In this work, the impact of an IL inserted between MoO_3 and the active film on the p-type transistor performance is studied. Bottom-gate and top-contact (BGTC) transistors based on amorphous 2,2′,7,7′-tetrakis(*N*,*N*-diphenylamino)-9,9-spirobifluorene (Spiro-TAD) and tris(4-carbazoyl-9-ylphenyl)amine (TCTA) as well as polycrystalline C8-BTBT were applied to reveal the device operation for OSCs with different film morphologies. For amorphous OSC thin film transistors, the insertion of the IL decreases SS and improves the effective mobility (μ_{eff}) due to reduced hole injection barrier.[16] In contrast, for polycrystalline C8-BTBT films, the insertion of an IL between the OSC and MoO_3 does not lead to clear improvements, which is ascribed to an inhomogeneous and discontinuous formation of the IL on the terrace-like C8-BTBT morphology dominated by distinct grain domains. These results demonstrate that the addition of a high-IE organic IL can provide efficient hole injection in OFETs, however under the condition that a homogenous and continuous interlayer is formed.

2. Results and Discussion

The schematic energy-band diagram in the top graph of **Figure 1**a illustrates the injection barrier at the interface between OSC and MoO_3. A high injection barrier (φ_b) occurs between MoO_3/Al and the active OSC layer.[14] At the MoO_3/OSC interface, a strong band bending is formed due to the charge transfer between MoO_3 and OSC. The Fermi level is pinned at deeper states in the broadened interface DOS, from which charges have to escape to the narrower bulk DOS, leading to an injection barrier. The band bending for increasing layer thickness is described well by including a Coulomb image potential due to differences in dielectric constants between MoO_3 and the organic semiconductor.[14] DOS broadening at the interface and the attractive image potential are the reason for the observed injection barriers at the metal-oxide contact. Insertion of an IL between MoO_3 and OSC can effectively realign the IE of the OSC and thus reduce the injection barrier, as shown in the bottom graph of Figure 1a.[14] To reveal the effect of IL on the hole injection for p-type OFETs, BGTC transistors were fabricated based on heavy doped silicon wafers with a 300 nm SiO_2 dielectric layer (Figure 1b). To reduce the interfacial traps at the dielectric OSC interface, the SiO_2 surface was modified by an octadecyltrichlorosilane (OTS) self-assembled monolayer applied by thermal vapor over 5 h. A 50 nm thick film of Spiro-TAD was thermally evaporated as active OSC layer followed by 5 nm thin TCTA as IL. The atomic force microscopy (AFM) images in Figure S1 in the Supporting Information display a featureless topography of the surface for both the OSC film and IL. Spiro-TAD has a moderate IE of 5.3 eV,[17] that is lower than the IE of TCTA (5.7 eV), consistent with the schematic displayed in Figure 1a.[18] MoO_3/Al was deposited subsequently as source and drain electrodes (Figure 1b). For comparison, reference OFETs without IL were also fabricated, using MoO_3/Al and Au contacts.

Transfer characteristics of the Spiro-TAD OFETs with IL/MoO_3/Al, MoO_3/Al, and Au contacts are shown in Figure 1c, and the corresponding output characteristics are presented in Figure S2 in the Supporting Information. The transistor with IL/MoO_3/Al contacts exhibits a low SS of 1.3 V dec^{-1} with a turn-on voltage around 0 V, whereas a SS of 3.0 V dec^{-1} for MoO_3/Al and 9.5 V dec^{-1} for Au contacts was derived. The gate-voltage dependences significantly differ between the three types of contacts. Especially for Au contacts, a nonlinear $I_{ds}{}^{1/2}$ behavior and a pronounced hysteresis in forward and backward scans (Figure S3a, Supporting Information) are observed, which are basically eliminated in the IL/MoO_3/Al configuration. These results demonstrate that the insertion of a TCTA IL improves the hole injection from MoO_3 into the active Spiro-TAD film. The μ_{eff} of Spiro-TAD OFETs is evaluated from linear and saturation regime in the transfer characteristics. As shown in Figure 1d, μ_{eff} of the IL/MoO_3/Al contact device is around 2.7–3.6 × 10^{-4} cm^2 V^{-1} s^{-1} with a low threshold voltage (V_T) of 0.1 V. In comparison, μ_{eff} and V_T for MoO_3/Al contact transistor are 0.9–1.1 × 10^{-4} cm^2 V^{-1} s^{-1} and −2.5 V, and for the device with only Au electrodes a high V_T of −21 V and a low μ_{eff} of 0.35–0.4 × 10^{-4} cm^2 V^{-1} s^{-1} were determined. This demonstrates that the insertion of a thin IL can efficiently increase μ_{eff} of Spiro-TAD OFETs.

The R_c and intrinsic charge carrier mobility (μ_{int}) of OFETs can be estimated using the transfer line method (TLM).[19] In the linear regime, the transistor ON resistance (R_{on}) can be written in terms of the channel resistance (R_{ch}) and R_c as

$$R_{on}(L) = R_{ch}(L) + R_c(L) = \frac{L}{\mu_{int} W C_i (V_G - V_T)} + R_c \quad (1)$$

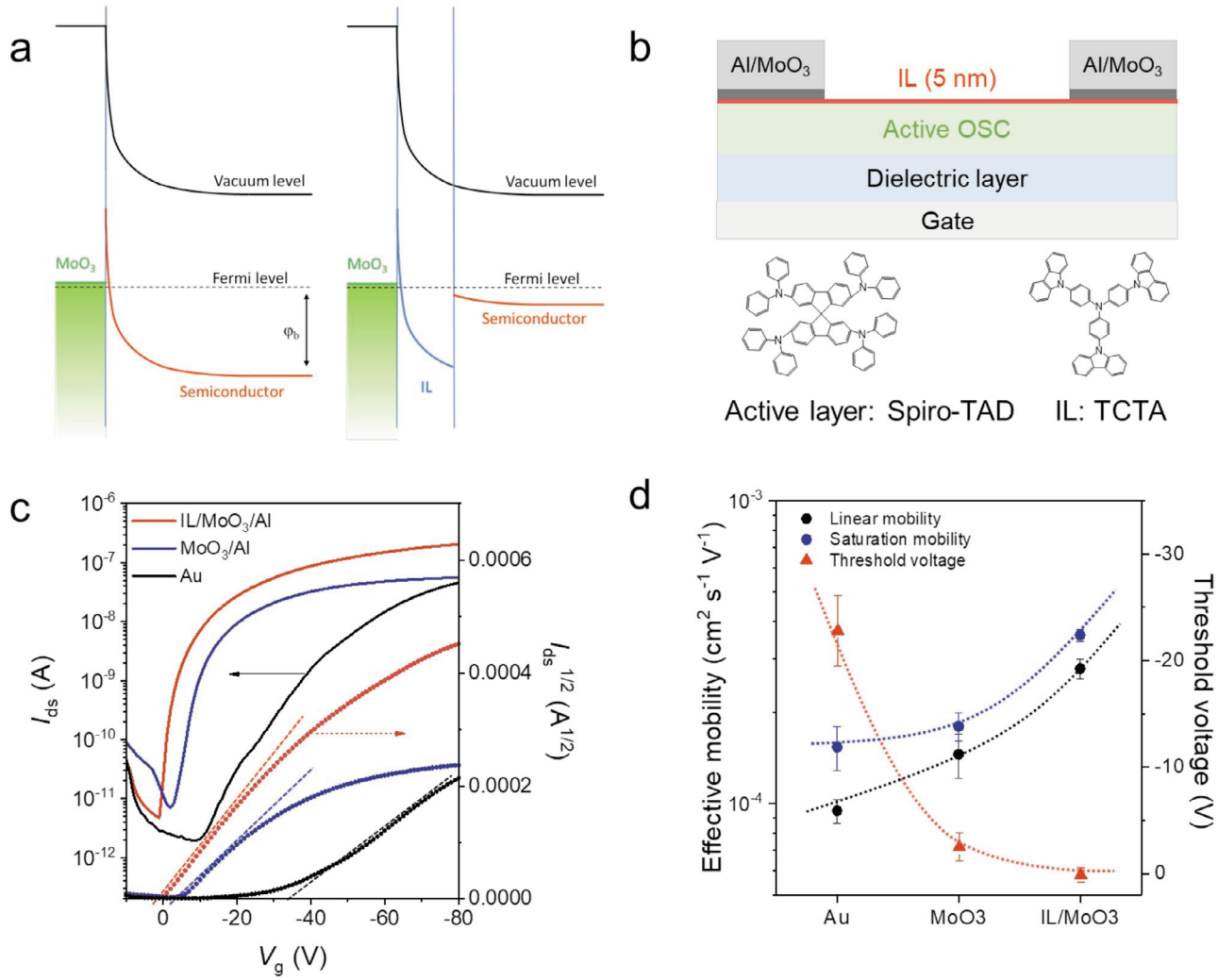

Figure 1. a) Schematic energy-band diagram indicating the injection barrier (φ_b) between MoO_3 and the active OSC layer. Introducing an IL of high IE realigns the IE of the organic semiconductor with the Fermi level. b) Schematic BGTC transistor configuration and the molecule structures of Spiro-TAD and TCTA. c) Transfer characteristics of Spiro-TAD OFETs with IL/MoO_3/Al, MoO_3/Al, and Au contacts. d) μ_{eff} and threshold voltage (V_T) of Spiro-TAD transistors with IL/MoO_3/Al, MoO_3/Al, and Au contacts.

where C_i is the capacitance of the dielectric layer, and L and W are the length and width of the transistor channel. In **Figure 2**a, the values of R_{on} normalized with respect to channel width, W, of the Spiro-TAD OFETs are plotted as a function of L for the device with IL/MoO_3/Al contacts. According to Equation (1), R_c and μ_{int} can be obtained from the y-intercept and slope of fitted line of R_{on}.[19] Channel-width-normalized R_{on} of MoO_3/Al and Au contact devices are presented in Figure S4 in the Supporting Information. As shown in Figure 2b, the variation in channel-width-normalized R_c with various gate voltages (V_g) (from –40 to –80 V) indicates a much lower R_c for the IL/MoO_3/Al device of around 7–15 × 10^6 Ω cm as compared to the MoO_3/Al (30–60 × 10^6 Ω cm) and Au contact transistors (100–250 × 10^6 Ω cm). The high R_c of the Au contact device mainly results from the injection barrier resulting from the energy difference in Au work-function (4.9 eV) and IE of Spiro-TAD (5.3 eV). Although MoO_3 has a higher work-function of around 6.7–7.0 eV, the corresponding OFET also exhibits a distinct R_c induced by the broadened DOS near MoO_3. Inserting an IL between Spiro-TAD and MoO_3 can decouple the electrode and OSC electrostatically and thus realign the Fermi level with the IE of OSC. In contrast to μ_{eff}, μ_{int} of around 8–9 × 10^{-4} cm^2 V^{-1} s^{-1} for Spiro-TAD-based OFETs is similar for the three different contacts since the insertion of IL did not influence neither the active OSC layer and nor the dielectric/OSC interface in the BGTC configuration. Consequently, the lower μ_{eff} for MoO_3/Al and Au contact devices directly results from a high R_c.

To prove the generality of the IL concept on improvement of the hole injection in OFETs, a 50 nm thick homogeneous TCTA film was vacuum evaporated as active layer on bare silicon/silicone dioxide substrate instead of OTS-modified substrate (Figure S5, Supporting Information). As IL, 5 nm thin 2,4,5,6-tetra(9*H*-carbazol-9-yl)isophthalonitrile (4CzIPN) was deposited (**Figure 3**a). The IE of 6.1 eV for 4CzIPN is higher than for TCTA (5.7 eV), satisfying the requirements for an efficient IL.[20] Transfer characteristics of TCTA OFETs prove that

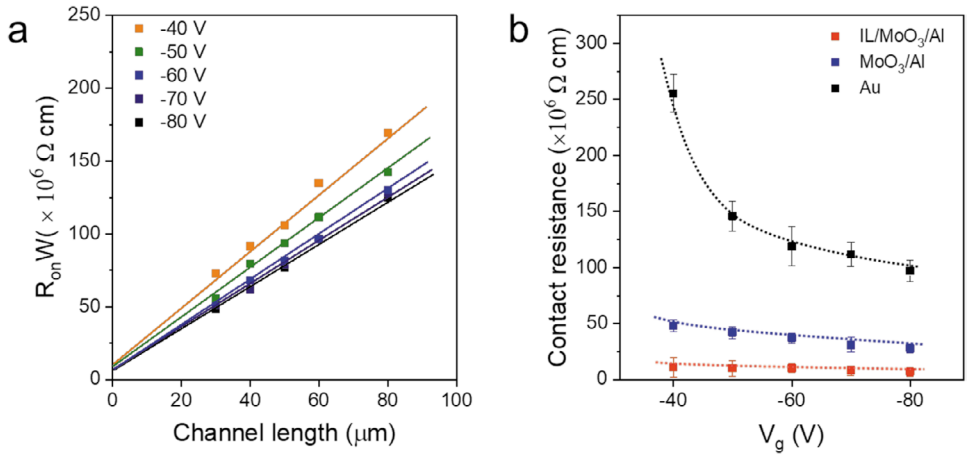

Figure 2. a) Channel-width-normalized R_{on} of Spiro-TAD OFETs with IL/MoO_3/Al contacts as a function of channel length (L) and at gate voltage (V_g) varied from −40 to −80 V (V_{ds}, −3 V), extracted for L between 30 and 80 μm and a channel width of 1000 μm. The y-intercepts of the fitted lines (solid lines) give the parasitic resistance at each V_g. b) Channel-width-normalized R_c for Spiro-TAD OFETs with IL/MoO_3/Al, MoO_3/Al, and Au contact as a function of V_g.

the insertion of IL between MoO_3 and TCTA also efficiently reduces SS, in this case from 11.6 to 3.5 V dec^{-1} (Figure 3b), and improves the operational device stability as evident from the ideal linear $I_{ds}^{1/2}$ curve and negligible hysteresis of the forward and backward scans (Figure S3b, Supporting Information). According to the transfer characteristics of the TCTA OFETs, the saturation μ_{eff} for IL/MoO_3/Al contacts is increased by three times in comparison to MoO_3/Al from 3.1×10^{-6} to 1.0×10^{-5} $cm^2\ V^{-1}\ s^{-1}$ (Figure 3c). The channel-width-normalized R_c of the TCTA OFETs with MoO_3/Al electrodes is 300–900 $\times$ 10^6 Ω cm, whereas the insertion of the 4CzIPN IL decreases R_c to 100–250 $\times$ 10^6 Ω cm. A μ_{int} of 7.5×10^{-5} $cm^2\ V^{-1}\ s^{-1}$ is

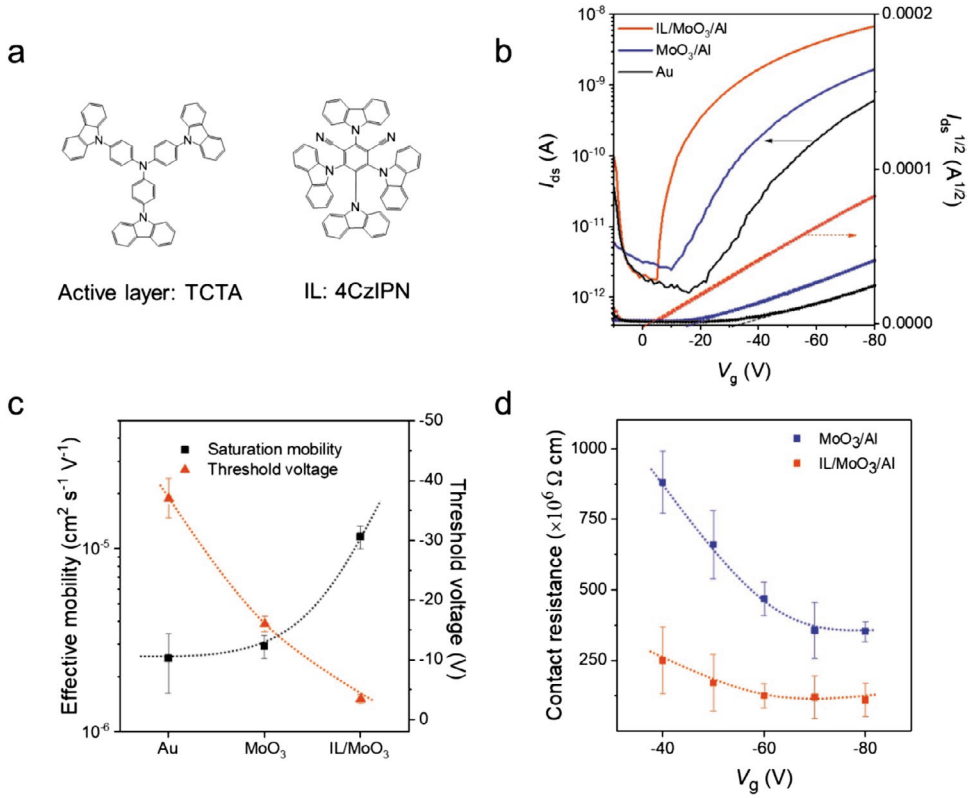

Figure 3. a) Molecule structures of TCTA and 4CzIPN. b) Transfer characteristics of TCTA OFETs with IL/MoO_3/Al, MoO_3/Al, and Au contacts. c) μ_{eff} and V_T of TCTA OFETs with IL/MoO_3/Al, MoO_3/Al, and Au contacts. d) Channel-width-normalized R_c of TCTA OFETs with IL/MoO_3/Al, MoO_3/Al, and Au contacts as a function of V_g.

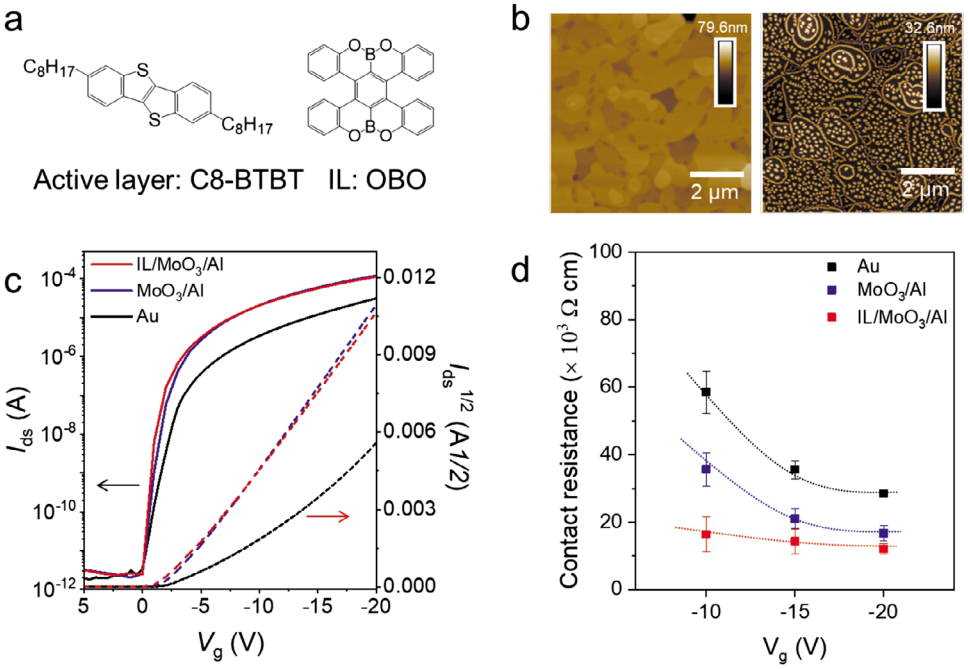

Figure 4. a) Molecular structures of C8-BTBT and OBO-bistetracene. b) AFM height images of C8-BTBT film and C8-BTBT/OBO-bistetracene bilayer. c) Transfer characteristics of C8-BTBT OFETs with IL/MoO_3/Al, MoO_3/Al, and Au contacts. d) Channel-width-normalized R_c of C8-BTBT OFETs with IL/MoO_3/Al, MoO_3/Al, and Au contacts as a function of V_g.

determined for the TCTA OFETs by TLM (Figure 3d; Figure S6, Supporting Information) and is also independent on R_c in this case. The high hole injection barrier in the Au contact TCTA OFETs results in a very low injection-limited current, insufficient for the TLM calculation.

Analogous to diodes,[14] this work has confirmed the concept of IL to enhance the hole injection in amorphous OSC thin film transistors. In comparison to amorphous OSC thin films, polycrystalline ones are also of great interest for OFETs since the high molecular order typically leads to high charge carrier mobility.[21,22] To study the impact of an IL on crystalline OSCs, C8-BTBT-based OFETs were fabricated (**Figure 4**a). The IE of C8-BTBT is about 5.7 eV, and OBO-doped tetrabenzo[*a*,*f*,*j*,*o*]perylene (OBO-bistetracene) was selected as IL due to its higher IE of around 5.9 eV.[23,24] First, a 50 nm thick C8-BTBT film was evaporated on an OTS-modified Si/SiO_2 substrate. AFM images in Figure 4b reveal a grain size of around 0.5–2.0 µm for the C8-BTBT film. The 5 nm thin OBO-bistetracene was deposited as IL on top of the crystalline C8-BTBT. Surprisingly, OBO-bistetracene nucleates as clusters only around the C8-BTBT domain boundaries of the terrace-like film surface as evident in the AFM image in Figure 4b. Transfer characteristics of C8-BTBT OFETs show in Figure 4c that MoO_3/Al contact devices exhibit a small SS of around 0.2–0.3 V dec^{-1}, which is lower than for the Au contact transistor (0.8 V dec^{-1}) as a result of the lower injection barrier (Figure S7, Supporting Information). The IL/MoO_3/Al and MoO_3/Al contact devices exhibit almost the same SS and a close μ_{eff} of around 3.0–3.3 $cm^2\ V^{-1}\ s^{-1}$ (Figure 4c). The insertion of the IL at the interface between C8-BTBT and MoO_3 leads only to a slight decrease in R_c as is evident from the channel-width-normalized graphs in Figure 4d. The limited effect of the IL on the charge injection into polycrystalline C8-BTBT OFETs is attributed to its aggregation on the terrace-like surface of the active film (right image of Figure 4b). A similar morphology was observed on C8-BTBT for other sublimated IL compounds (Figure S8, Supporting Information). Therefore, a homogenous and continuous morphology of IL is a prerequisite for an effective reduction of the hole injection barrier in p-type OFETs.

3. Conclusion

In OFETs with high IE OSCs, the high work-function MoO_3 electrode exhibits limited injection into amorphous active films. To overcome this limitation, the combination of MoO_3 with an interlayer with high ionization energy provides a universal strategy to efficiently inject hole charge carriers into amorphous OSC films as used in OFETs. In comparison to MoO_3/Al electrodes, the insertion of IL in amorphous Spiro-TAD and TCTA thin film transistors significantly improves the injected hole current and effective charge carrier mobility by reducing R_c. The decrease of the injection barrier by an IL is rationalized by decoupling the electrode from the organic semiconductor, preventing electrostatic barrier formation at the OSC/electrode interface. A higher IE and a homogeneous and continuous morphology of the interlayer are the critical requirements for reducing R_c and enhancing hole injection in organic electronics.

4. Experimental Section

Materials: C8-BTBT, Spiro-TAD, TCTA, and OTS were purchased from Sigma-Aldrich and used without further purification. 4CzIPN was

Received: December 4, 2019
Revised: March 10, 2020
Published online:

synthesized according to the procedure described in the literature[20] and purified by vacuum sublimation. OBO-bistetracenes was synthesized according to the procedure described in the literature.[24] Silicon substrates with a 300 nm thick SiO_2 layer were treated by oxygen plasma for 3 min. The OTS self-assembled monolayers were obtained by exposing the silicon wafers to the corresponding silane vapor at 150 °C for 6 h.

Morphology Characterization: Film thickness measurements were performed by a KLA Tencor Profiler and a Bruker Dimension Icon FS AFM. The film morphology was characterized a Bruker Dimension Icon FS AFM in tapping mode.

Charge Transport Characterization: A bottom-gate and top-contact configuration was employed for OFET devices. The heavily doped n-type Si wafers were used as gate electrode and the 300 nm thick SiO_2 layer (capacitance of 11 nF cm^{-2}) was adopted as a gate dielectric layer. The active OSC and IL layers were deposited by thermal evaporation in glove-box to reduce the influence of water and oxygen, respectively. For Au contact devices, source and drain electrodes were deposited at a thickness of 50 nm. For MoO_3/Al contact devices, source and drain electrodes were deposited by 10 nm MoO_3 followed by 100 nm Al in sequence. The transistor channel width was 1000 µm and the channel length varied from 30 to 80 µm. A Keithley 4200-SCS was used for all standard electrical measurements in glove-box under nitrogen atmosphere.

Supporting Information

Supporting Information is available from the Wiley Online Library or from the author.

Acknowledgements

K.Z. thanks the China Scholarship Council (CSC) for financial support. T.M. acknowledges the Foundation for Polish Science financed by the European Union under the European Regional Development Fund (POIR.04.04.00-00-3ED8/17-01). W.P. acknowledges National Science Centre, Poland, through the grant UMO-2015/18/E/ST3/00322. The authors thank Prof. Yutaka for the synthesis of compound 4CzIPN.

Conflict of Interest

The authors declare no conflict of interest.

Keywords

charge-carrier injection, contact resistance, electrode interlayer, organic field-effect transistors, organic semiconductors

[1] H. Sirringhaus, *Adv. Mater.* **2014**, *26*, 1319.
[2] H. Dong, X. Fu, J. Liu, Z. Wang, W. Hu, *Adv. Mater.* **2013**, *25*, 6158.
[3] S. Wang, P. Gao, I. Liebewirth, K. Kirchhoff, S. Pang, X. Feng, W. Pisula, K. Müllen, *Chem. Mater.* **2011**, *23*, 4960.
[4] T. He, M. Stolte, C. Burschka, N. H. Hansen, T. Musiol, D. Kälblein, J. Pflaum, X. Tao, J. Brill, F. Würthner, *Nat. Commun.* **2015**, *6*, 5954.
[5] C. Liu, Y. Xu, Y. Y. Noh, *Mater. Today* **2015**, *18*, 79.
[6] G. Heimel, L. Romaner, E. Zojer, J. L. Bredas, *Acc. Chem. Res.* **2008**, *41*, 721.
[7] K. Y. Wu, S.-Y. Yu, Y.-T. Tao, *Langmuir* **2009**, *25*, 6232.
[8] B. de Boer, A. Hadipour, M. M. Mandoc, T. van Woudenbergh, P. W. M. Blom, *Adv. Mater.* **2005**, *17*, 621.
[9] B. Lüssem, M. L. Tietze, H. Kleemann, C. Hoßbach, J. W. Bartha, A. Zakhidov, K. Leo, *Nat. Commun.* **2013**, *4*, 2775.
[10] T. Minari, P. Darmawan, C. Liu, Y. Li, Y. Xu, K. Tsukagoshi, *Appl. Phys. Lett.* **2012**, *100*, 093303.
[11] M. Kröger, S. Hamwi, J. Meyer, T. Riedl, W. Kowalsky, A. Kahn, *Appl. Phys. Lett.* **2009**, *95*, 123301.
[12] Kano, T. M , K. Tsukagoshi, *Appl. Phys. Lett.* **2009**, *94*, 143304.
[13] A. Ablat, A. Kyndiah, G. Houin, T. Y. Alic, L. Hirsch, M. Abbas, *Sci. Rep.* **2019**, *9*, 6685.
[14] N. B. Kotadiya, H. Lu, A. Mondal, Y. Ie, D. Andrienko, P. W. M. Blom, G. A. H. Wetzelaer, *Nat. Mater.* **2018**, *17*, 329.
[15] W. Mönch, *Semiconductor Surfaces and Interfaces*, 2nd ed., Springer Series in Surface Science, Vol. *26*, Springer-Verlag, Berlin **1995**.
[16] J. Dong, P. Yu, S. A. Arabi, J. Wang, J. He, C. Jiang, *Nanotechnology* **2016**, *27*, 275202.
[17] R. A. Belisle, P. Jain, R. Prasanna, T. Leijtens, M. D. McGehee, *ACS Energy Lett.* **2016**, *1*, 556.
[18] R. T. White, E. S. Thibau, Z. H. Lu, *Sci. Rep.* **2016**, *6*, 21109.
[19] T. Minari, Y. Miyata, M. Terayama, T. Nemoto, T. Nishinaga, K. Komatsu, S. Isoda, *Appl. Phys. Lett.* **2006**, *88*, 083514.
[20] H. Uoyama, K. Goushi, K. Shizu, H. Nomura, C. Adachi, *Nature* **2012**, *492*, 234.
[21] X. T. Zhang, H. L. Dong, W. P. Hu, *Adv. Mater.* **2018**, *30*, 1801048.
[22] Z. F. Yao, J. Y. Wang, J. Pei, *Cryst. Growth Des.* **2018**, *18*, 7.
[23] R. Janneck, N. Pilet, S. P. Bommanaboyena, B. Watts, P. Heremans, J. Genoe, C. Rolin, *Adv. Mater.* **2017**, *29*, 1703864.
[24] X. Y. Wang, A. Narita, W. Zhang, X. Feng, K. Müllen, *J. Am. Chem. Soc.* **2016**, *138*, 9021.

